Phase Sensitivity and Entrainment in a Modeled Bursting Neuron

S. S. Demir,* R. J. Butera, Jr.,* A. A. DeFranceschi,* J. W. Clark, Jr.,* and J. H. Byrne†
*Department of Electrical and Computer Engineering, Rice University, Houston, Texas and †Department of Neurobiology and Anatomy, University of Texas Medical School, Houston, Texas USA

ABSTRACT A model of neuron R15 in *Aplysia* was used to study the mechanisms determining the phase-response curve (PRC) of the cell in response to both extrinsic current pulses and modeled synaptic input and to compare entrainment predictions from PRCs with those from actual simulations. Over the range of stimulus parameters studied, the PRCs of the model exhibited minimal dependence upon stimulus amplitude, and a strong dependence upon stimulus duration. State-space analysis of the effect of transient current pulses provided several important insights into the relationship between the PRC and the underlying dynamics of the model, such as a correlation between the prestimulus concentration of Ca^{2+} and the poststimulus phase of the oscillation. The system nullclines were also found to provide well-defined limits upon the perturbatory extent of a hyperpolarizing input. These results demonstrated that experimentally applied current pulses are sufficient to determine the shape of the PRC in response to a synaptic input, provided that the duration of the current pulse is of a duration similar to that of the evoked synaptic current. Furthermore, we found that predictions of phase-locked 1:*m* entrainment from PRCs were valid, even when the duration of the periodically applied pulses were a significant portion of the control limit cycle.

INTRODUCTION

Analyses of phase sensitivity in biological systems date back to Brown and Eccles (1934), who showed that the effects of brief bursts of vagal nerve activity depended on their time of occurrence within the cardiac cycle. This study led to numerous experimental investigations of phase sensitivity and entrainment in the heart (Dong and Reitz, 1970; Guevera et al., 1988; Jalife and Moe, 1976; Levy et al., 1969; Reid, 1969; Weidmann, 1951), and the same perturbation techniques have been applied to the study of a number of other biological systems (Aschoff, 1965; Glass and Mackey, 1988; Pavlidis, 1973). These studies have revealed that biological oscillators frequently exhibit a phasic dependency of the effect of a perturbation on the oscillation. Depending on the timing of the perturbation, the period of the current cycle of the oscillation may be advanced or delayed. Furthermore, the phase sensitivity of an oscillator to an external perturbation has been found to be a criterion for the oscillator to be entrained by repeated application of the perturbation (Enright, 1965; Perkel et al., 1964). Thus the phase sensitivity and entrainment properties of biological oscillators appear to be related measures of an oscillator's response to external input. Pinsker (1977a, b), showed that endogenous neuronal bursting oscillators in *Aplysia* also exhibit phase sensitivity to brief perturbations. Regardless of the stimulus type (neurally released transmitter or a depolarizing or hyperpolarizing current pulse), the brief perturbations altered the cycle length of oscillation by an amount that depending on the timing, amplitude, and duration of the input.

Although the parametric aspects of phase sensitivity and entrainment have been analyzed extensively, little is known about the biophysical mechanisms that endow biological oscillators with these properties. In the present study we examine the biophysical mechanisms of phase sensitivity and entrainment by using a model of neuron R15 in *Aplysia* (Butera et al., 1995) as a representative model of a typical endogenously bursting neuron. We extended the model of Butera et al. (1995) to incorporate an inhibitory synaptic current. We investigated the phasic response of the model to transient inhibitory current pulse inputs of varying amplitude and duration. Phase-response curves and phase-transition curves were generated and related to transient responses in the state space, which were then correlated with the modeled biophysical mechanisms. The phasic sensitivity of the model to synaptic inputs and extrinsic hyperpolarizing pulses was compared. We found that for a given synaptic input there existed a current pulse input with similar response characteristics. Finally, we studied the entrainment properties of the model cell to both current pulse and synaptic input, and related these properties to the phase-response curves.

Received for publication 29 April 1996 and in final form 10 October 1996.

Dr. Demir's present address is School of Biomedical Engineering, University of Tennessee, Memphis, TN.

Dr. Butera's present address is Mathematical Research Branch, NIDDK, National Institutes of Health, Bethesda, MD.

Address reprint requests to Dr. J. W. Clark, Jr., Department of Electrical and Computer Engineering, Rice University, P.O. Box 1892, Houston, TX 77251-1892. Tel.: 713-527-8101, X3597; Fax: 713-524-5237; E-mail: jwe@ece.rice.edu.

0006-3495/97/02/579/16 $2.00

MODEL DEVELOPMENT

The membrane model

We used a recently developed model of neuron R15 in *Aplysia* (Butera et al., 1995), which consists of 12 state variables, including membrane potential, intracellular con-

centration of Ca^{2+}, intracellular concentration of cAMP, Ca^{2+} buffer occupancy, and eight voltage-dependent state variables. The model adequately simulates bursting activity, beating activity, and silent behavior as the stimulus current (I_{stim}), the concentration of serotonin (5-HT), or the concentration of dopamine (DA) are modified. The model also simulates the rather unique responses of R15 to current pulses in the presence of 5-HT or DA.

In this study the complete model is identical to that published by Butera et al. (1995), with the addition of a synaptic current I_{syn}. For all simulations no modulatory agents are applied and [cAMP] is at a steady-state concentration of 1 μM. Several changes in notation were made. For simplicity the variable c is used to represent the concentration of intracellular Ca^{2+} in all mathematical expressions. In addition, the term $I_{NS,Ca}$ represents the portion of the I_{NS} current (described shortly) carried by Ca^{2+} ions.

The differential equations describing the activity of the model are

$$\frac{dV}{dt} = \frac{-(I_{spike} + I_{sub} - I_{STIM} + I_{syn}(V, g_{syn}))}{C_m}$$

$$\frac{dc}{dt} = \frac{\begin{bmatrix} I_{NaCa}(V, c) - I_{CaP}(c) - I_{SI}(V, c, s) \\ - I_{Ca}(V, d, f, c) - I_{NS,Ca}(V, b, c) \end{bmatrix}}{2Vol_i F} \quad (1)$$

$$- n[B]_i \frac{dO_C}{dt} \quad (2)$$

$$\frac{dO_C}{dt} = k_U c(1 - O_C) - k_R O_C$$

$$I_{spike} \equiv I_{Na}(V, m, h) + I_{Ca}(V, d, f, c) + I_K(V, n, l) + I_{NS}(V, b, c) \quad (3)$$

$$I_{sub} \equiv I_{SI}(V, c, s) + I_R(V) + I_L(V) + I_{NaCa}(V, c) + I_{CaP}(c) + I_{NaK}(V)),$$

where V is the membrane potential, c is the concentration of intracellular Ca^{2+}, and O_C is the occupancy of the intracellular Ca^{2+} buffer. I_{spike} is defined as the sum of those currents that are active only during the firing of action potentials, whereas I_{sub} is defined as the sum of those currents responsible for the subthreshold oscillations underlying bursting activity. I_{STIM} is the applied stimulus current and I_{syn} is the modeled synaptic current (described below). The model also consists of eight Hodgkin-Huxley-type gating variables (h, m, d, f, s, b, n, l) whose differential equations are of the form

$$\frac{dz}{dt} = \frac{z_\infty(V) - z}{\tau_z(V)}. \quad (4)$$

The entire set of equations for the model is provided in the Appendix.

A detailed description of the ionic currents and their gating variables may be found in Butera et al. (1995). Briefly, I_{Na} and I_K are responsible for the upstroke and repolarization of the action potential, respectively. I_{Ca} is an inward Ca^{2+} current that is activated on the repolarizing phase of each action potential and is responsible for the majority of Ca^{2+} influx associated with each action potential. I_{NS} is a nonspecific low-amplitude current with slow kinetics that is only active during the firing of action potentials. None of the currents comprising I_{spike} are active at subthreshold potentials (below approximately -40 mV). I_{SI} is the current that is responsible for bursting activity. It is activated by a voltage-dependent gating variable s and inactivated by c. The steady-state activation curve of s increases between -60 mV and -20 mV and is a half-maximum at -40 mV. The time-constant of s is voltage-dependent and is typically between 0.2 and 1.0 s. I_R is an anomalous rectifying potassium current. It is instantaneous and active at potentials below -40 mV. I_L is a leakage current. I_{NaCa}, I_{CaP}, and I_{NaK} are the Na^+-Ca^{2+} exchanger, Ca^{2+}-extrusion pump, and Na^+-K^+ exchanger, respectively.

The synaptic model

Our study does not focus upon the physiological role of R15 (see Alevizos et al., 1991, for a review) but rather treats the modeled R15 as a representative endogenously bursting neuron, drawing upon the wealth of experimental and modeling information on R15 (for a review see Adams and Benson, 1985). This study is an initial step in ongoing experimental and modeling studies of the pattern-generating properties of recurrent inhibition networks of bursting cells with recurrent inhibition. Thus we were only concerned with inhibitory inputs. One of our goals was to compare the phase sensitivity of the model to inhibitory synaptic input with that of extrinsically applied current pulses. This is of experimental importance, because in vitro it is easier to apply external current pulses than to activate a synaptic input.

The equation for synaptic current is of the form

$$I_{syn} = g_{syn}(V - E_{syn}), \quad (5)$$

where g_{syn} is the macroscopic conductance of the synaptic channel, V is the membrane potential, and E_{syn} is the reversal potential of the synaptic channel. E_{syn} was set to -77 mV (E_K) to ensure that the synaptic current was inhibitory.

To formulate an equation for synaptic conductance, g_{syn}, we assumed that the binding of the transmitter to the synaptic channel is rapid compared to the time scale of the conformational change of the synaptic channel, consistent with the findings of Gardner and Stevens (1980) in the buccal ganglion of *Aplysia*. Using these assumptions, we developed the following equation to describe the time rate of change of g_{syn}, which is similar to equation 9a of

Magleby and Stevens (1972):

$$\frac{dg_{syn}}{dt} = -k_r g_{syn} + k_f \bar{g}_{syn} \frac{[T]_c}{K_M + [T]_c}, \quad (6)$$

where k_r is the rate constant of the closing of the synaptic channel, k_f is the rate constant of the opening of the synaptic channel, $\bar{g}_{syn}$ is the maximum conductance of the synaptic channel, and K_M is the half-maximum concentration of transmitter buildup in the synaptic cleft. We assumed that transmitter concentration in the cleft does not approach saturation and set K_M at 2 M. The forward rate constant k_f was set at 12 ms^{-1}, and the constants $\bar{g}_{syn}$ and k_r were set to various values to achieve a peak conductance of 0.65 μS (Gardner and Stevens, 1980) with varying synaptic durations. These values are specified in the Results.

The above equation requires a change in transmitter concentration to effect a change in g_{syn}. For all simulations involving I_{syn}, we used a predefined transmitter waveform (Fig. 6 *A*) that was derived by 1) using our model of R15 as a model of a presynaptic burst, 2) assuming that transmitter release into the synaptic cleft was proportional to I_{Ca} of the presynaptic cell, and 3) assuming that decay of transmitter was fast relative to the inactivation kinetics of the synaptic channel (i.e., the transmitter decays at a rate much faster than k_r.

System nullclines

Previous analyses of our model have shown that the burst cycle is governed by two variables that operate on a much slower time scale than those associated with the generation of the action potential. These variables are the voltage-dependent activation of the slow inward current (s) and the intracellular concentration of Ca^{2+} (c). We previously exploited the difference in time scales by treating c and s as parameters and analyzed the resulting reduced model (Butera et al., 1996). Two conclusions are important for the analysis of transient responses in the (c, s) state space (Butera et al., 1996):

1. The (c, s) phase space can be split into two regions, one in which action potentials fire at a given value of (c, s), and one in which the cell remains silent. The line separating these two regions can be calculated and is hereafter referred to as L. (For details on the calculation of L, refer to Butera et al., 1996.)
2. When the model lies in the silent region of (c, s) space, the dynamics reduce to a second-order system of c and s with all other state variables (including membrane potential) at quasi-steady-state values.

These two conclusions permit us to utilize nullclines of the slow variables c and s to examine the phasic responses of hyperpolarizing current pulses. With all state variables except c and s set to their steady-state values at a given value of (c, s), the system nullclines are numerically calculated as those values of (c, s) such that $ds/dt = 0$ (the s nullcline) or $dc/dt = 0$ (the c nullcline).

COMPUTATIONAL METHODS

Temporal integration of all differential equations was accomplished using an implicit fifth-order Runga-Kutta method with variable step size designed for stiff systems of differential equations (Hairer and Wanner, 1990). Calculation of the c and s nullclines was accomplished using PITCON (Rheinboldt and Burkardt, 1983a, b), a numerical continuation program that tracks the fixed solutions of a systems of equations as a free variable is varied. Computation of the boundary of the subthreshold region of state space (mathematically, a two-parameter continuation of a saddle node bifurcation) was performed using AUTO (Doedel, 1981), a bifurcation analysis package that solves for fixed and periodic solutions of a system of differential equations as one or two system parameters are varied. Full details on the calculations of the nullclines and saddle node bifurcation may be found in Butera et al. (1996). All time-dependent simulations were written in the C programming language, except for the numerical integration method, which was written in FORTRAN. All numerical analysis code (using routines of PITCON or AUTO) was written in FORTRAN. All code was run on Sun Microsystems Sparc-series workstations.

The numerical integration of the model utilizes a variable step size, and care was taken to ensure that the model did not integrate across time points at which discrete changes in parameters (for example, turning on a current pulse stimulus) took place. Each call to the integrator was made for a time period in which the parameters remained fixed.

Phase-response curves (PRCs) were constructed by plotting the relative change in period ($\Delta P/P_0$) versus the normalized phase of a single applied stimulus, where P_0 is the free-running (control) cycle length and ΔP is the change in the length of the period ($P_1 - P_0$) in response to an applied hyperpolarizing stimulus. This change in period length is illustrated in Fig. 1. In each simulation the transient input was applied t_s seconds after the beginning of the burst cycle, which is defined as the time at which the upstroke of the first action potential of burst crosses −40 mV. The response time (t_r) is defined as the time from the beginning of the stimulus to the beginning of the next burst ($P_1 = t_s + t_r$, the duration of the test cycle in which the stimulus was applied).

Entrainment curves were calculated by applying a periodic stimulus to the model. The model's activity was determined to be phase-locked to the input when successive values of t_s were less than 0.01 s apart. The model was considered to be nonconvergent at a given stimulus frequency if convergence did not occur within 100 cycles. Successive values of t_s were also compared with values 2 and 3 cycles past to identify 2:m or 3:m entrainment, respectively. Entrainment simulations were performed for a

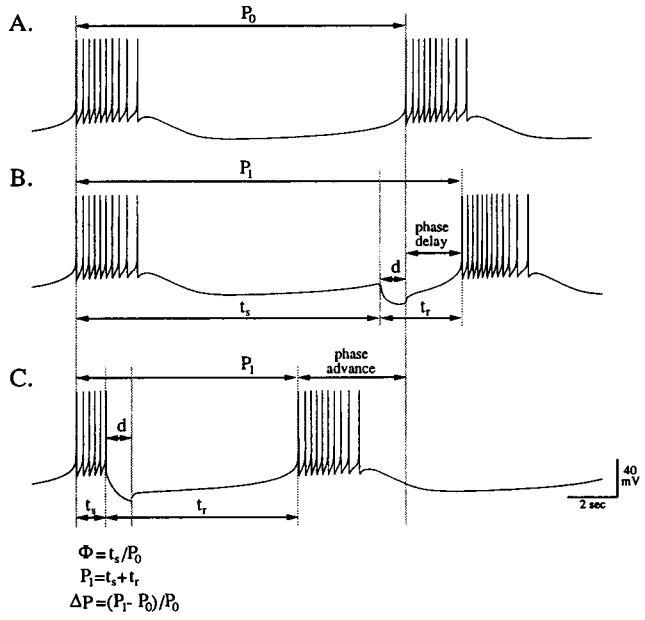

FIGURE 1 Phase sensitivity of the modeled neuron to a transient input. (*A*) Changes in membrane potential in the absence of input. The burst cycle has a length of P_0 seconds. (*B* and *C*) Effects on the burst cycle of a hyperpolarizing current pulse applied t_s into the burst cycle. A new burst begins t_r s after application of the pulse. *B* illustrates phase delay, where the perturbed cycle length (P_1) is longer than the control cycle (positive ΔP). *C* illustrates phase advance, where the perturbed cycle length (P_1) is shorter than the control cycle (negative ΔP). The phase of the stimulus application is defined as Φ, and *d* is the duration of the stimulus in seconds.

range of periods and input durations and represented as entrainment diagrams, which plot the entrainment ratio *n*:*m* as a function of stimulus period and duration. The entrainment ratio *n*:*m* signifies *m* cycles of the bursting oscillation for every *n* cycles of the input stimulus.

RESULTS

Model review

For values of I_{STIM} between −0.55 nA and 1.55 nA the model exhibits a stable limit-cycle oscillation that is characterized as bursting. For all simulations in this study, I_{STIM} = 0.0 nA in the absence of a perturbational stimulus. For this value of I_{STIM} the model has a control period (P_0) of 13.26 s. The temporal and phasic trajectories of the burst cycle are illustrated in Fig. 2. Panels *A1–A3* illustrate the time course of membrane potential (*V*), intracellular concentration of Ca^{2+} (*c*), and the voltage-dependent activation (*s*) of the slow inward (I_{SI}) Ca^{2+} current, respectively. The burst trajectory in the state space of the two slow variables, *c* and *s*, is illustrated in Fig. 2 *B*. The dashed line *L* marks the boundary between the "silent" and "firing" regions of the model in the (*c*, *s*) state space (Butera et al., 1996) and is essentially the action potential threshold in terms of *c* and *s*. The (*c*, *s*) state space view of the burst cycle will be utilized in future sections to analyze the phasic effects of transient stimuli.

The burst occurs as the two slow variables *c* and *s* traverse the state space back and forth across *L*. Both of these variables regulate a key subthreshold current I_{SI} that governs the burst cycle. I_{SI} is activated by *s* and inactivated by *c*. During the hyperpolarized interval between bursts of action potentials, Ca^{2+} is removed from the cell via pumps and exchangers (Fig. 2 *B*, *point 1*). Eventually enough Ca^{2+} is removed from the cell to significantly remove the Ca^{2+} inactivation of I_{SI}, such that sufficient inward current now exists to depolarize the cell (Fig. 2 *B*, *point 2*). As the cell gradually depolarizes, I_{SI} is regeneratively voltage-activated via *s*, and eventually enough subthreshold inward current exists to elicit a sustained firing of action potentials (Fig. 2 *B*, *point 3*). Each action potential causes additional Ca^{2+} influx into the cell (Fig. 2 *B*, *point 4*). This Ca^{2+} influx gradually inactivates I_{SI} and activates I_{CaP} (the Ca^{2+} extrusion pump) until the total amount of subthreshold current is

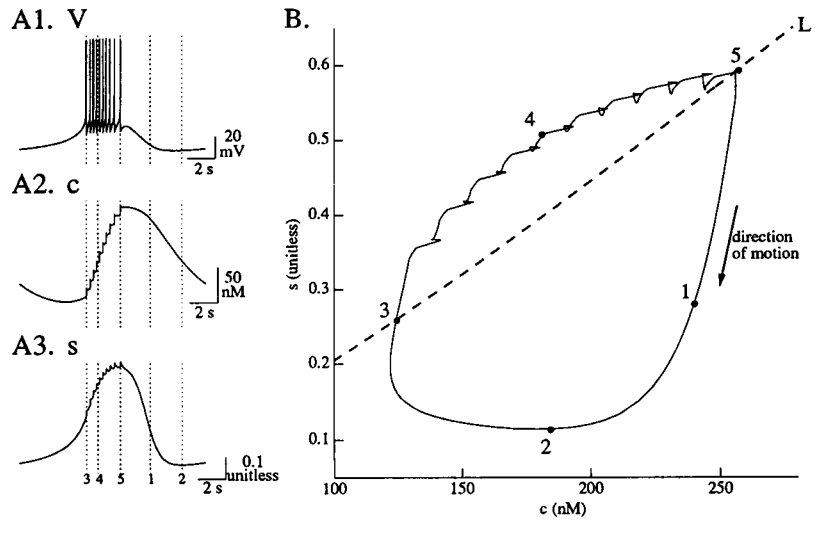

FIGURE 2 The control burst cycle in the absence of modulatory or I_{STIM} input. (*A1–A3*) Time course of membrane potential (*V*), intracellular concentration of Ca^{2+} (*c*), and activation of I_{SI} (*s*) over one burst cycle. Vertical dotted lines labeled 1–5 correspond to time points identified in the (*c*, *s*) state space (*B*) (*c*, *s*) state space illustration of the burst cycle. Dashed line labeled *L* represents the threshold above which fixed values of (*c*, *s*) will result in the model firing action potentials.

no longer net inward, and consequently action potentials can no longer be supported (Fig. 2 *B*, *point 5*). At this point the cell hyperpolarizes, further reducing I_{SI} via the deactivation of s, and the burst cycle repeats itself (Fig. 2 *D1*).

Phase analysis

Phase-response curves

The phase sensitivity of the model to hyperpolarizing current pulses of varying duration and amplitude is illustrated in Fig. 3. Fig. 3 *A* shows the burst cycle over a normalized cycle length. Fig. 3 *B1* illustrates the PRCs for a hyperpolarizing current pulse with constant duration (1 s) and changing amplitude (1.6, 2, 5, and 10 nA). We found that 1.6 nA was the minimum amplitude required for a 1-s pulse to interrupt the burst and hyperpolarize the cell at any phase in the burst cycle. Fig. 3, *C1* and *D1*, illustrates the PRCs for a hyperpolarizing current pulse with constant amplitude (5 nA) and varying duration (0.3, 0.5, 1, 2, 3, 5, and 10 s). Fig. 3, *B2*, *C2*, and *D2*, illustrates in (c, s) space the control limit cycle (*C*), and the perturbed limit cycle (Glass and Mackey, 1988) for each PRC is shown in Fig. 3, *B1*, *C1*, and *D1*. The perturbed limit cycle is defined as the locus of all new states reached immediately after the stimulus has been removed. These plots provide insight into which slow variables are affected by the transient stimulus and will be considered when we discuss the effect of pulse duration on the PRCs in a later section.

Each PRC and perturbed limit cycle consists of 200 data points. Each data point corresponds to an individual simulation where a transient input was applied t_s seconds into the limit cycle, where $t_s = (i/200)P_0$, $i = 0 \ldots 199$. The PRCs exhibit spike-like discontinuities during the burst phase. These discontinuities correspond to the coincidence of a stimulus with the upstroke of an action potential and are only evident because of the high resolution with which the PRC is generated. Such discontinuities are a by-product of the two very different time scales evident in bursting cells. The action potentials are approximately 20 ms in duration and elicit currents several hundred nA in magnitude, whereas the burst cycle is 13.26 s long and involves subthreshold currents typically less than 5 nA in magnitude. Thus, for the range of stimulus amplitudes investigated in this study, there exist small windows of time (approximately 10 ms) at the upstroke of each action potential in the burst where the effect of an inhibitory current pulse is diminished by the fast inward current I_{Na}.

On initial glance, the PRCs appear to be nonperiodic. However, the PRCs, regardless of a choice of reference point, obey the relationship $f(P_0) = f(0) + 1$, so the PRCs are periodic in a modulo sense (i.e., the end points correspond to perturbations to the same phase in the burst cycle). It will be shown shortly that the corresponding phase-transition curves are periodic.

For discussion purposes we divided the phase ($\Phi = t_s/P_0$) into three distinct intervals labeled I, II, and III. These intervals are indicated in Fig. 3 *B1*, but are defined in a similar way for Fig. 3, *C1* as well. Interval I ($0 \leq \Phi < 0.2$) corresponds to the duration of the burst. A pulse applied in

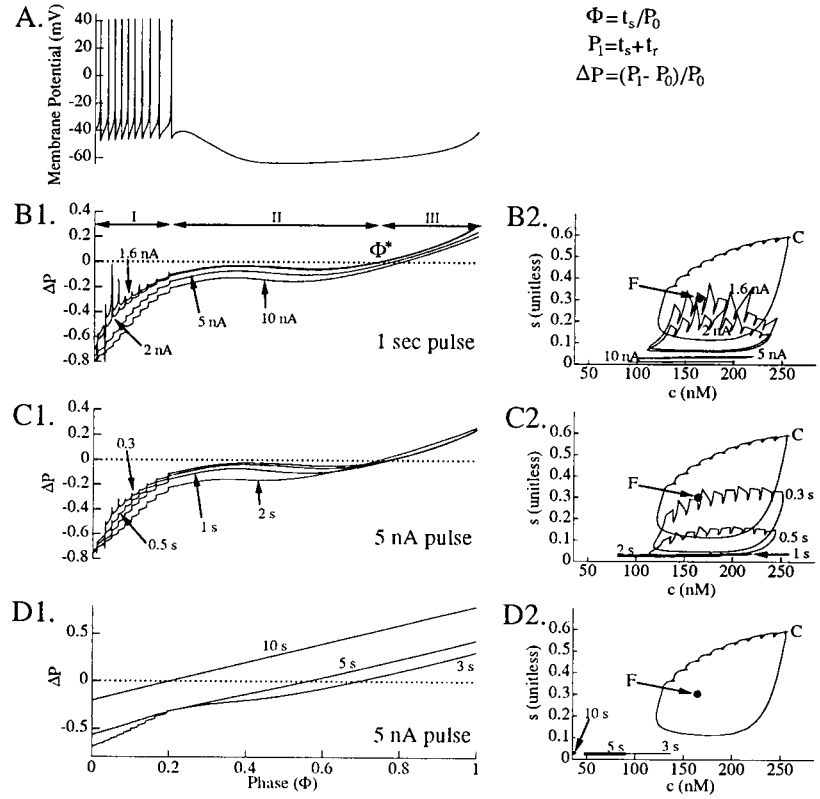

FIGURE 3 Phase-response curves (PRCs) of the model in response to hyperpolarizing current pulses of varying magnitudes and durations. (*A*) Membrane potential of the control cycle. (*B1*) PRCs of the model to 1 s hyperpolarizing current pulses of 1.6 nA, 2 nA, 5 nA, and 10 nA. Φ* indicates the approximate location of the critical phase (no phase shift). Roman numerals indicate qualitative labeling of the three distinct regions of the PRC. (*C1*) PRCs of the model to a 5-nA pulse of 0.3, 0.5, 1, and 2 s. (*D1*) PRCs of the model to a 5-nA pulse of 3, 5, and 10 s. (*B2–D2*) The perturbed limit cycles to the same inputs used to generate the PRCs of *B1–D1*, respectively. The control limit cycle is labeled *C*, and the equilibrium point is labeled *F*. Some of the perturbed limit cycles in *C2* and *D2* overlap and are highlighted in bold to differentiate them. See text for the methodology used to obtain the PRCs and perturbed limit cycles.

this interval significantly shortened the cycle length, as shown by the negative values in the PRC. Interval II ($0.2 \leq \Phi < \Phi^*$) corresponds to the relatively flat region of the PRC extending from the end of the burst to the critical phase (Φ^*). The critical phase is defined as the point where the PRC crosses the 0 axis (Φ^*) and signifies the location in the cycle at which a perturbational pulse generates no change in cycle length. A pulse applied in interval II shortened the overall burst cycle to a small degree (much smaller than pulses applied during interval I). Interval III ($\Phi^* \leq \Phi < 1$) corresponds to the region in which the PRC takes on positive values. A pulse applied in this region prolonged the length of the current cycle.

The effects of changes in stimulus amplitude (A) for a fixed-duration current pulse (1 s) are illustrated in Fig. 3 *B1* for stimuli in the range 1.6 nA $\leq A \leq$ 10 nA. The only effects of increasing amplitude upon the PRC were a slight shift of the curve downward and a corresponding positive shift in Φ^* over the range $0.73 \leq \Phi^* \leq 0.80$. Although amplitude was varied over a significant range (as high as 20 nA; not shown), the general shape of the PRC remained the same.

The effects of changes in the stimulus duration (D) using a fixed amplitude (5 nA) are illustrated in Fig. 3, *C1* and *D1*, for stimuli in the range of 0.3 s $\leq D \leq$ 2 s and 3 s $\leq D \leq$ 10 s, respectively. Changes in the duration over the range 0.3 s $\leq D <$ 1 s shifted the PRC slightly downward over intervals I and II, with virtually no change in the PRC or in Φ^* in interval III ($0.76 \leq \Phi^* \leq 0.77$). For $D \geq 2$ s, there were two pronounced effects: Φ^* was displaced strongly to the left and intervals II and III merged, so that the PRC gradually became piecewise linear, with a steeper slope during interval 1 (3-s pulse; Fig. 3 *D1*). At very long stimulus lengths, the PRCs became linear (10-s pulse; Fig. 3 *D1*). For longer pulses the duration of the perturbational signal was large and represented a significant fraction of the control period P_0.

Phase-transition curves

Phase-transition curves (PTCs) are an alternative form of describing the phase-response characteristics of the modeled neuron and contain the same information as the PRC, only displayed in a different manner. The PTC is a plot of the poststimulus phase (Ψ) versus the prestimulus phase (Φ). Most studies consider the stimulus duration to be short and the phase transition to be instantaneous, and define $\Psi = 1 - t_r/P_0$ (Clay et al., 1990; Glass and Mackey, 1988; Pavlidis, 1973; Perkel et al., 1964). However, in the present study the stimulus is sometimes a significant portion of the burst cycle, so we define $\Psi = 1 - (t_r - d)/P_0$, where d is the duration of the stimulus.

Fig. 4 *B* illustrates the PTCs for 5-nA stimuli of varying durations (1, 3, 5, and 10 s). Fig. 4 *A* illustrates the membrane potential of the control burst cycle for comparison. The PTCs show that for shorter pulses the poststimulus phase varied significantly with the prestimulus phase. However, for longer pulse durations the PRC was nearly constant

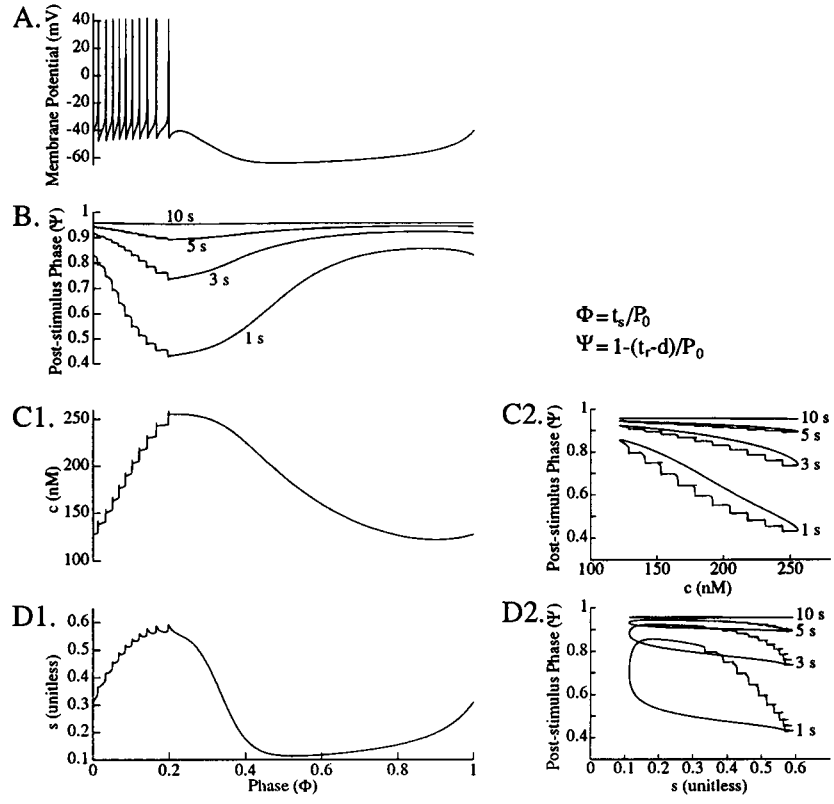

FIGURE 4 Phase-transition curves (PTCs) of the model in response to a 5-nA hyperpolarizing current pulse of varying durations. (*A*) Membrane potential of the control cycle, (*B*) PTC, a plot of poststimulus phase (Ψ) versus prestimulus phase (Φ), where t_r is the time from the pulse application to the next burst, d is the pulse length, and P_0 is the duration of the control cycle (all in seconds). Labels indicate the PTCs for pulses 1, 3, 5, and 10 s in duration. (*C1*) Values of c (concentration of intracellular Ca^{2+}) during the control cycle. (*C2*) Plot of Ψ versus prestimulus value of c (data in *B* versus data in *C1*). (*D1*) Values of s (activation of I_{SI}) during the control cycle. (*D2*) Plot of Ψ versus prestimulus value of s (data in *B* versus data in *D1*).

in Ψ, indicating phase-independent resetting (i.e., the burst recurred within a fixed time interval after the stimulus has been turned off, regardless of the phase of stimulus application). The nearly constant PTCs associated with longer-duration current pulses (5, 10 s) correspond to linear PRCs (Fig. 3 *D*). Fig. 4, *A*, *C1*, and *D1*, illustrates how the variables associated with I_{SI}, namely, the membrane potential (V), the intracellular concentration of Ca^{2+} (c), and the voltage-dependent activation variable (s) change within the control cycle. A comparison of the shapes of the PTCs in Fig. 4 *B* with the variables plotted in Fig. 4, *A*, *C1*, and *D1*, suggests that the PTCs (especially for the shorter duration stimuli) are similar in shape to the waveform of c. Fig. 4, *C2* and *D2*, illustrates Ψ versus the prestimulus values of c and s (i.e., the data of Fig. 4 *B* versus Fig. 4, *C1* and *D1*), respectively. Ψ has a nearly monotonic relationship with c, whereas there are considerable dynamic differences between Ψ and s over the time course of the burst cycle. Thus, there is a strong correlation between the prestimulus concentration of intracellular Ca^{2+} and the resulting poststimulus phase of the oscillation. The correlation of Ψ with c (rather than s) reflects the difference between the time scales of c and s. Although both variables are described as "slow" variables (with respect to the time scale of the action potential), c is about an order of magnitude slower than s (i.e., c changes on a time scale of tens of seconds, whereas s changes on a time scale of 0.2–1 s). The relationship between the prestimulus values of c and the PTC points to the underlying cellular mechanisms that are responsible for phase sensitivity and will be explored in greater detail in the following section.

The results illustrated in Figs. 3 and 4 show that for the range of stimulus parameters considered in this study, stimulus amplitude has a minimal effect on the shape of the PRC, whereas stimulus duration evokes significant changes in the PRC. Results similar to those in Fig. 3, *C1* and *D1*, were also obtained with current pulses of other magnitudes (2 nA and 10 nA). Furthermore, the correlation between Ψ and c at the time of stimulation was found to be valid for pulses of lesser magnitude (as low as 2 nA) or duration (as short as 0.3 s). Ψ is nearly constant for pulses longer than 5 s (for magnitudes from 1.6 to 10 nA), indicating phase-independent resetting, whereas pulses shorter than 5 seconds still possess nonlinear PRCs. Although the stimulus pulse may have a duration that represents a significant fraction of the burst cycle (5 s is 38% of P_o), it still has nonlinear perturbational effects.

PRCs of other types of input

All of the PRCs discussed thus far exhibit strong (type 0) resetting (see Discussion). This is the type of PRC typically exhibited by the bursting neurons L3 (Pinsker, 1977a) and R15 (H. Lechner, D. Baxter, and J. Byrne, unpublished observations) in vitro and thus was the primary focus of this study. The model possesses distinctly different PRCs in response to inputs of smaller amplitude and/or shorter duration (not shown) than those just discussed. The PRCs to smaller or shorter inputs are typically type 1, exhibiting a relatively uniform phase delay during the burst portion of the limit cycle and an apparent discontinuity at the end of the burst phase. The remainder of the PRC is similar in shape to those of Fig. 3 *B1*. As the intensity or duration of the stimulus is increased, the location of the discontinuity shifts toward a location earlier in the burst phase, with the PRC to the left of the discontinuity exhibiting relatively uniform delay and the PRC to the right of the discontinuity similar to those of Fig. 3 *B1*. When this discontinuity shifts to $\Phi = 0$, the PRC makes a transition from type 1 to type 0.

We found that the PRCs in the response to depolarizing current pulses were typically type 0, even for relatively weak pulses (as low as 1 nA, 0.5 s). These PRCs possessed a small amount of phase delay for the first half of the burst cycle, a sharp increase in phase delay around $\Phi = 0.6$ (approximately the minimum membrane potential of the burst cycle), and a relatively even amount of phase delay after the rise. As the stimulus intensity or duration was increased, the first half of the PRC became more linear and increased in slope, reducing the extent of the sharp rise at $\Phi = 0.6$. For pulses large enough in amplitude or duration, the two halves of the PRC merged into one smooth curve. For example, the PRC in response to a 5-nA, 1-s depolarizing pulse looks similar in shape to the PRC of Fig. 3 *D1*) (−5 nA, 3 s), only shifted upward.

State space analysis of the PRC

The transient responses studied in the previous section were examined in the (c, s) state space to investigate the ionic basis of the cellular dynamics associated with the three intervals of the phase-response curve. The (c, s) state space was chosen because previous work (Butera et al., 1996) has shown that bursting is regulated by the two slow variables c and s, and that during the interburst interval (and any other time that the cell is hyperpolarized and not firing action potentials) the model dynamically collapses to a system of the two variables c and s (all other variables are near steady state).

We chose to examine in the (c, s) state space the effects of 5-nA hyperpolarizing current pulses of varying durations applied at three different locations during the burst cycle corresponding to the three intervals of the PRC identified previously. Because time is not evident on state space diagrams, the location of the trajectory at intervals of 10% of the cycle (1.33 s) is indicated by the labeled circles in Fig. 5 *A*. The pulses were applied during the burst cycle at $t_s = 1$ s ($\Phi = 0.075$, interval I), $t_s = 4$ s ($\Phi = 0.30$, interval II), and $t_s = 11$ s ($\Phi = 0.83$, interval III). In all of the state space diagrams of Fig. 5, time increases as trajectories are followed in a clockwise direction. Fig. 5, *B–D*, illustrates the response of the model in the (c, s) state space to 5-nA pulses of varying durations applied during intervals I, II,

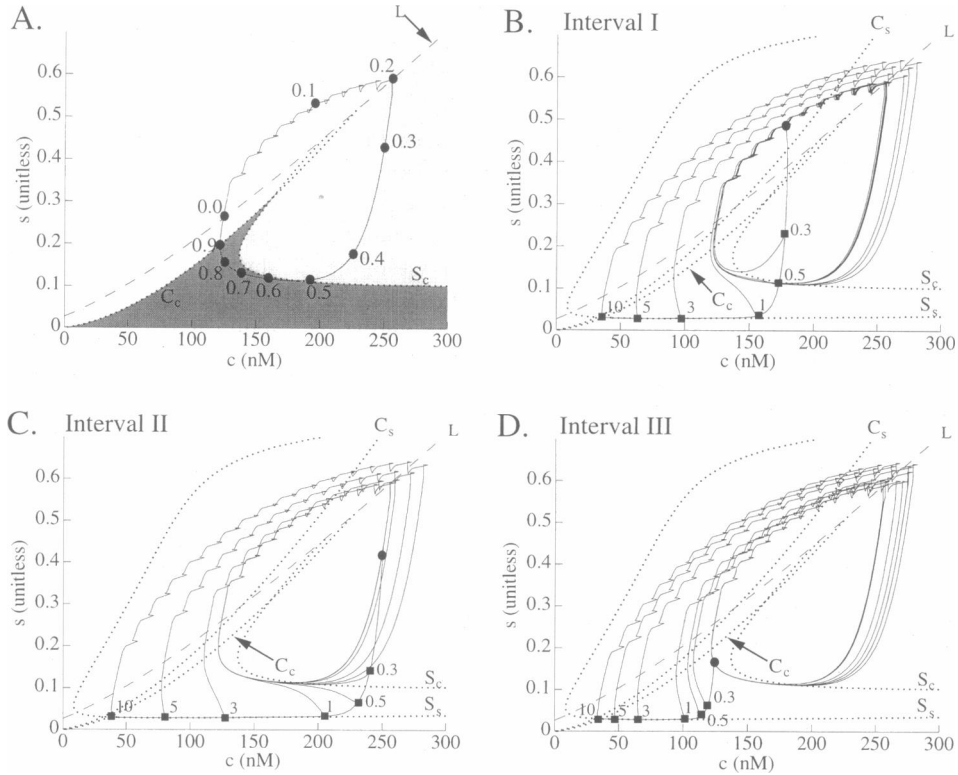

FIGURE 5 Phase space examination of 5-nA pulses of varying durations applied during intervals I, II, and III. For all panels, the control burst cycle in (c, s) space is indicated in bold. The c and s nullclines of the model in the absence of input are dotted and labeled C_c and S_c, respectively. The c and s nullclines of the model during application of a 5-nA hyperpolarizing pulse are dotted and labeled C_s and S_s, respectively. The dotted line L indicates the action potential threshold in (c, s). (*A*) Labeled circles indicate evenly spaced points in time along the control burst cycle. Each point corresponds to a 0.1 change in phase (1.33 s). See text for a description of shading. (*B–D*) Phase space trajectories of various duration current pulses applied 1 s (*B*), 4 s (*C*), and 11 s (*D*) into the limit cycle. Circles indicate point at which stimulus was applied. Squares indicate point at which stimulus was removed. Label next to square indicates duration of stimulus.

and III, respectively. In these panels the time point of stimulus delivery is marked by a solid circle and the time point of stimulus release is marked by a solid box labeled with a number indicating the duration of the applied stimulus in seconds. Also shown on Fig. 5, *B–D*, are the c and s nullclines for $I_{STIM} = 0$ nA and $I_{STIM} = -5$ nA (*dotted lines*) and the line L, which is equivalent to an action potential threshold in (c, s) space. When the solution trajectory in (c, s) is "below" L, the dynamics of the model collapse to a second-order system in (c, s) (Butera et al., 1996). When the solution trajectory is "above" L in (c, s), higher-order processes become active and action potentials fire. We refer to the c and s nullclines for $I_{STIM} = 0$ nA as the control nullclines and use the notations S_c and C_c, respectively. Likewise, we refer to the c and s nullclines for $I_{STIM} = -5$ nA as the stimulus nullclines and use the notations S_s and C_s, respectively. Thus the control nullclines graphically describe the governing equations of the solution trajectory in the absence of a stimulus, whereas the stimulus nullclines graphically describe the governing equations of the solution trajectory during application of the stimulus.

The system nullclines divide (c, s) into three major regions, which are indicated by the shading in Fig. 5 *A*. In the white region, c and s are always increasing. This region includes all of (c, s) above L. In the light-shaded region, c and s are always decreasing. In the dark-shaded region, c is always decreasing, and s is increasing. These three regions divide the limit cycle into approximately the three intervals of the PRC identified in Fig. 3. There is a small region near the location where S_c and C_c cross, where c is increasing and s is decreasing. However, this region is so small relative to the other regions that it is not considered in our dynamic analysis.

The responses of the model to a 5-nA stimulus of varying durations applied during interval I are shown in Fig. 5 *B*. This is the interval where the phase-response curve shows the most significant region of phase advance (Fig. 3, *B1* and *C1*). The current pulse immediately hyperpolarizes the membrane, causing a voltage-dependent decrease in s. The trajectory crosses L, eliminating the possibility of the firing of action potentials upon removal of the pulse. Whereas short pulses only decrease s, longer pulses decrease c as well. This decrease in c occurs as the solution trajectory meets S_s and continues along the nullcline, decreasing in c and gradually moving toward the stable fixed point located at the intersection of S_s and C_s. The significant amount of phase advance encountered during this interval occurs because the perturbation advances the trajectory clockwise toward the latter portion of the limit cycle oscillation. The limit cycle corresponding to $0.45 < \Phi < 0.85$ is approximately parallel to the S_s nullcline.

Pulses applied in interval II (Fig. 5 *C*) have the effect of slightly advancing the phase (Fig. 3 *C2*). As in interval I, short pulses cause a decrease in s, with longer pulses causing a decrease in c as well. Pulses 1 s or longer reach S_s and continue along the nullcline (decreasing in c) until the stimulus is removed. The advance in phase due to pulses applied during interval II is not significant, because the perturbation only slightly hastens the solution trajectory in the "intended" direction of the limit cycle. For example,

perturbations that move the trajectory to S_s continue decreasing in c, in a direction parallel to that of the unperturbed limit cycle.

Pulses applied during interval III delay the onset of the next burst (Fig. 3 *B1* and *C1*). As in the preceding two intervals, short pulses cause a decrease in s toward S_s, and longer pulses continue the trajectory along S_s, decreasing in c. Short perturbations applied in this interval move the trajectory away from L, prolonging the time until the next burst. Longer perturbations (>1 s) move the trajectory farther away from the limit cycle, delaying the onset of the following burst because of the length of the perturbation.

Ionic basis of the PRC

During hyperpolarization the model dynamically collapses to two variables, s and c, with all other variables (including V) at quasi-steady-state (Butera et al., 1996). Thus those ionic currents that strongly regulate the activity of the model at hyperpolarized potentials should be subthreshold currents that are dependent upon these two variables. Only three currents are dependent on c and/or s and are active at subthreshold potentials. One of these currents, I_{SI}, is largely responsible for the bursting oscillations. The other currents are the Ca^{2+} extrusion pump (I_{CaP}), which is activated by c, and the Na^{+}-Ca^{2+} exchanger (I_{NaCa}), which is Ca^{2+}- and V-dependent.

These three currents also determine dc/dt (I_{Ca} and I_{NS} are inactive at hyperpolarized potentials). Recall that C_c denotes all points in (c, s) where $dc/dt = 0$, thus marking the boundary in (c, s) between Ca^{2+} influx and Ca^{2+} efflux. Any perturbation that moves the solution trajectory 1) below L, and 2) to a location positive in c to C_c, will result in a negative dc/dt upon removal of the perturbation. Thus any hyperpolarizing pulse of a magnitude sufficient to interrupt the burst should cause the cell to initially extrude Ca^{2+} upon removal of the pulse. Examining Fig. 5, it would be expected that a solution perturbed at a high value of c would take longer to recross L (which marks the approximate beginning of a burst) than a solution perturbed at a lower value of c, because the trajectory after the perturbation would be further away from C_c. This expectation is in agreement with the data of Fig. 4 *C2*, which shows a correlation between prestimulus values of c and the poststimulus phase of the oscillation, a measure of the time until the beginning of the next burst.

It is difficult to assess the dynamical contribution of the Ca^{2+}-dependent currents to the voltage drive of the model. I_{SI} is net inward, increasing with s, and decreasing with c. I_{CaP} is net outward, increasing with c. I_{NaCa} is inward at hyperpolarized potentials, with its magnitude increasing as c decreases. At hyperpolarized potentials, V is at quasi-steady state and the model is dynamically a function of two variables, c and s. However, V is still implicitly a function of those two variables, and there are other voltage-dependent currents whose magnitudes vary throughout the state space. The nullclines of the slow variables provide some information on whether the membrane is hyperpolarizing or depolarizing in different regions of the state space. This information on the membrane potential can be related to our previously defined regions of the PRC. Under the assumption that V is at quasi-steady state, the rate of change of membrane potential is given by

$$\frac{dV}{dt} = \frac{dV}{ds}\frac{ds}{dt} + \frac{dV}{dc}\frac{dc}{dt}. \tag{7}$$

By inspection of figure 2 of Butera et al. (1996), dV/ds is always positive and dV/dc is always negative in the region of state space occupied by the limit cycle. Thus any region in the state space where $ds/dt > 0$ and $dc/dt < 0$, $dV/dt > 0$. Therefore, we know that any trajectory perturbed into this region results in a depolarizing membrane potential and corresponds to interval III of the limit cycle. This region of the state space is shown by the dark shaded region in Fig. 5 *A*.

Magnitude, duration, and phase resetting

The changes in s and c due to current pulse perturbations are limited in (c, s) by C_s and S_s. The location of the lower branch of S_s is determined by the magnitude of the stimulus pulse. Pulses shorter than 1 s will be perturbed in the negative s direction toward S_s, whereas pulses longer than 1 s will be perturbed to (but not past) S_s. Once the solution trajectory reaches S_s, the duration of the stimulus pulse determines the extent of the perturbation of the solution in the negative c direction. The effects of extremely long pulses are limited by the location of fixed point defined by the intersection of C_s and S_s. For such long pulses, phase-independent resetting occurs.

Relaxation times

The use of the PTC as an estimate of the phase of the cycle after removal of the stimulus is built upon the assumption that the perturbed trajectory converges to the control limit cycle before the beginning of the next burst (where the period measurement is made). Examination of the results of Fig. 5, *B–D*, shows that this assumption is valid for perturbations that do not shift c below its minimum during the control cycle ($c_{min} \approx 120$ nM). This includes hyperpolarizing pulses 1 s or less in duration applied during most of intervals I and II ($0 < \Phi < 0.65$), and excludes any hyperpolarizing pulse applied during interval III. Pulses that violate this criterion yield a trajectory that converges to the control limit cycle after the following burst. The burst following the perturbation is typically longer than the control case, with more action potentials during the burst. Thus there is a certain degree of error in utilizing the PTC information as prediction of the degree of the phase transition due to a transient stimulus. However, the fact that convergence occurs after no more than one limit cycle suggests that this error may be minimal. The degree of this error will be studied shortly when the PRC is utilized as a

predictive measure of the response of the model to entrainment by a periodically applied stimulus.

Synaptic inputs

We next investigated the phase sensitivity of the model to inhibitory synaptic input. The predefined transmitter waveform is illustrated in Fig. 6 *A*. The impulse-like features of the synaptic waveform are consistent with our assumption that there is no significant buildup of transmitter in the cleft with a train of pulses and emphasize the fact that the summation of pulses occurs because of channel kinetics. We considered four different synaptic models driven by the transmitter waveform in Fig. 6 *A*. The parameters for these four models are listed in Table 1 and are described in terms of the length of the activation of g_{syn} in response to the transmitter waveform: brief (shorter than the burst—only the first second of the transmitter waveform is used), short (the length of the burst), medium, and long (the length of the entire burst cycle). The synaptic conductance waveforms for the four models are illustrated in Fig. 6 *B*. The PRCs of the model for each of the four synapses are illustrated in Fig. 6 *C*. For each synaptic model, the parameters were adjusted so that the peak conductance is the same. Qualitatively, the relationship between the shape of the PRCs and the synaptic duration is similar to that found earlier for the length of a current pulse (compare with Fig. 3, *C* and *D*). The mechanistic behavior of the ionic membrane currents in response to transient synaptic input may also be analyzed in (*c*, *s*) space, as was shown previously for externally applied hyperpolarizing current pulses (Fig. 5). Because the synaptic input exerts its effect by activating a hyperpolarizing current, the responses are similar to those of Fig. 5 and are not shown.

Although the time course of I_{syn} was not rectangular (as with I_{STIM}), we found that it was possible to utilize current pulse inputs to obtain PRCs similar to those obtained by synaptic inputs. For example, the PRCs in response to the brief and long synaptic inputs compared favorably with the

TABLE 1 Parameters used for synaptic conductance kinetics of varying durations

Type	$\bar{g}_{syn}$ (μS)	k_r (ms^{-1})
Brief	7.00	0.0020
Short	6.50	0.0020
Medium	3.45	0.0007
Long	2.65	0.0004

k_r was set to achieve the desired decay length, then $\bar{g}_{syn}$ was adjusted to achieve a peak conductance of 0.65, μS. Brief, Short, Medium, and Long correspond to the waveforms labeled B, S, M, and L in Fig. 6 *B*.

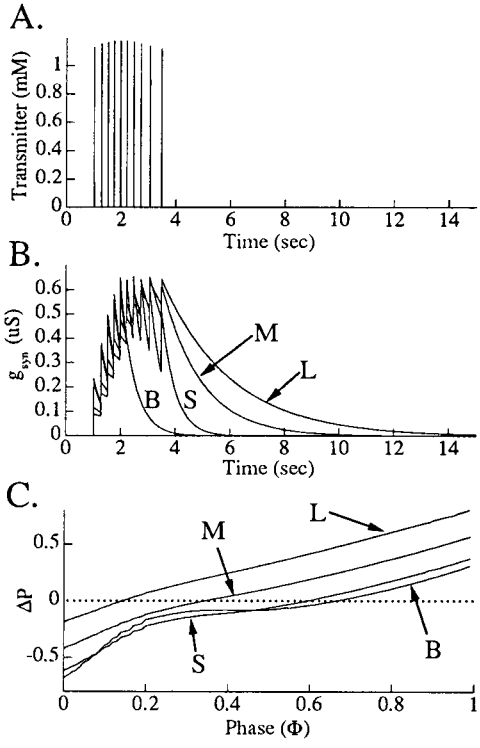

FIGURE 6 Effects of differing channel kinetics with identical maximum conductances. (*A*) Time course of predefined transmitter waveform. (*B*) Time course of g_{syn} for the four different synaptic channel models identified in Table 1. The brief synaptic model (*B*) only used the first second of the transmitter waveform. (*C*) PRCs of the cell model using the four different synaptic channel models.

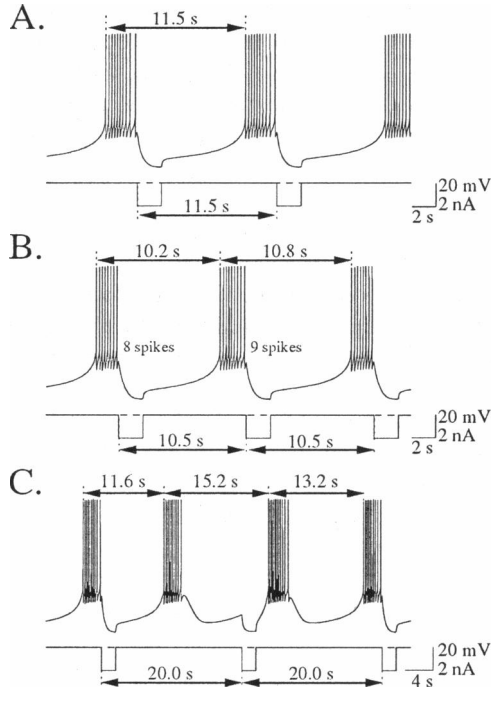

FIGURE 7 Examples of entrainment to a 2-nA, 2-s hyperpolarizing current pulse. Current pulses were continuously applied to the model with periods of 11.5 s (*A*), 10.5 s (*B*), and 20.0 s (*C*). (*A*) The model entrained to a 1:1 relationship with the input stimulus. (*B*) The model entrained to a 2:2 relationship with the input stimulus. The burst phase alters between eight and nine action potentials. (*C*) The model exhibits three burst periods of distinct lengths for every two cycles of the stimulus.

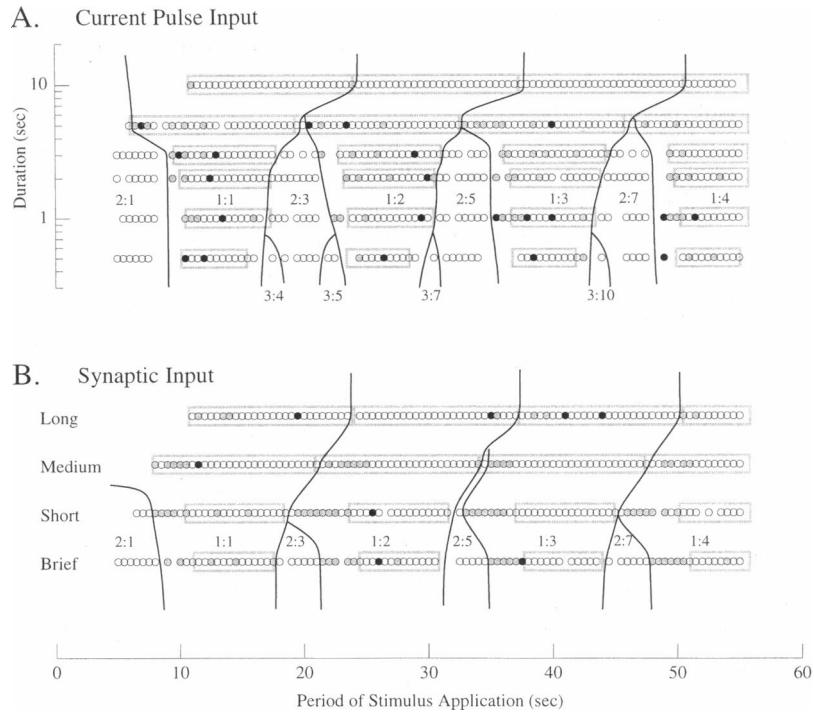

FIGURE 8 Simulated and predicted entrainment zones for current pulse (*A*) and synaptic (*B*) input. In *A* the hyperpolarizing current pulses were 2 nA in magnitude and 0.5, 1, 2, 3, 5, and 10 s in duration. The synaptic inputs in *B* correspond to the parameters sets listed in Table 1. Each circle represents stable entrainment between a periodically applied stimulus and the model. The hand-drawn black lines identify the entrainment zones, which are labeled *n*:*m*, signifying *n* cycles of the stimulus input for every *m* cycles of the period of the modeled neuron. The gray and black filled circles in the 1:*m* entrainment zones identify simulations in which 2:2*m* and 3:3*m* entrainment, respectively, were found. The gray boxes in the 1:*m* entrainment zones indicate the ranges of 1:*m* entrainment predicted by the PRC for the corresponding input.

PRCs in response to 2-nA hyperpolarizing current pulses 2 s and 10 s in length, respectively. Given our finding that duration of input (pulse or synaptic) is a key parameter affecting the shape of the PRC, we conclude that experimentally applied current pulses are sufficient to determine qualitatively the range of shapes of PRCs that may be elicited by an inhibitory synaptic input.

Entrainment curves

We next examined the response of the model to periodic stimulation. Two issues were considered: 1) how well do the PRCs predict the entrainment of the model, and 2) how well do current pulses entrain the model, compared to synaptic input with a similar PRC? The inputs were the current pulse and synaptic inputs of brief and long duration corresponding to the PRCs discussed in the previous section.

Entrainment simulations

Entrainment occurs when repetitive application of an input to an oscillator causes the oscillator to exhibit periodic behavior that is in synchrony with the forcing oscillator. The character of the synchronous relationship between the periodic input and the forced oscillator may take many forms, however. Entrainment is typically characterized by the ratio *n*:*m*, representing *n* cycles of the stimulus for every *m* cycles of the forced oscillator (Glass and Mackey, 1988). Fig. 7 *A* illustrates 1:1 entrainment exhibited by the model when a 2-nA, 2-s hyperpolarizing current pulse is applied to the model every 11.5 s. After a brief transient period, the model is also entrained to a period of 11.5 s.

For some periods of stimulation the model exhibited multiphasic periodicity, where the model phase-locked to two or three alternating values of t_s on successive applications of the input pulses. Fig. 7, *B* and *C*, shows two examples of 2:*m* entrainment. Fig. 7 *B* illustrates the steady-state response of the model in response to a 2-nA, 2-s hyperpolarizing current pulse applied every 10.5 s. The model alternates between a period of 10.8 s and a period of 10.2 s (note the difference in the number of action potentials in each burst). Such entrainment is referred to as 2:2 entrainment, because for every two cycles of input the model exhibits two distinct burst periods. Fig. 7 *C* illustrates the steady-state response of the model in response to a 2-nA, 2-s hyperpolarizing current pulse applied every 20 s. In this case the model exhibits 2:3 entrainment (i.e., for every two current pulses applied every 20 s, the model exhibits three distinct burst periods of 11.6 s, 13.2 s, and 15.2 s).

Fig. 8 illustrates the zones of entrainment as a function of stimulus period and stimulus duration. Fig. 8 *A* illustrates the entrainment zones found in response to current pulse inputs of various duration. Fig. 8 *B* illustrates the entrainment zones found in response to the four types of synaptic input previously described. Each circle indicates a simulation for which phase-locked entrainment was identified. The solid black lines (hand-drawn) separate the zones of entrainment. In the 1:*m* entrainment zones, the gray and black filled circles indicate, respectively, simulations for which 2:2*m* or 3:3*m* entrainment was identified. The gray rectangular boxes in the 1:*m* entrainment zones indicate the extent of the entrainment zone predicted by the PRC for each type of input studied. The calculation of these predicted zones of entrainment will be discussed shortly. The structure of the

entrainment diagrams as stimulus duration is decreased is similar to the Arnold tongue structure exhibited by many oscillatory systems as the amplitude duration is increased (Glass and Mackey, 1988).

In the 1:1 entrainment zone, the model is capable of being entrained at periods shorter than its fundamental period as well as periods longer than its fundamental period. Entrainment at periods other than the fundamental period is only possible if the PRC possesses regions of phase advance and phase delay, respectively. The more pronounced the degree of phase advance and phase delay in the PRC, the wider the regions of entrainment in the PRC. The existence of entrainment zones other than 1:1 shows that for stimulus periods significantly shorter or longer than P_0, the model entrains at a superharmonic or subharmonic, respectively, of the control period. The existence of discrete entrainment zones suggest that there exist upper and lower bounds on the range of periods for which a given entrainment ratio may be exhibited. These findings are consistent with the experimental findings of Perkel et al. (1964) on *Aplysia* beating neurons.

Entrainment predictions

We utilized the method of Perkel et al. (1964) to predict the extent of the integer (1:m) zones of entrainment. First we consider the case of 1:1 entrainment. Let $f(t_s)$ represent the unnormalized PRC (i.e., $P_1 = P_0 + f(t_s)$). The following two conditions define upper and lower boundaries upon τ, the period of entrainment, where 1:1 phase locking may occur:

$$\tau > P_0 + \min(f(t_s)) \tag{8}$$

$$\tau < P_0 + \max(f(t_s)), \tag{9}$$

where t_s, the unnormalized phase in the burst cycle where the periodic stimulus arrives, is given by $t_s = f^{-1}(\tau - P_0) = \Phi P_0$. Because of the shape of all of the PRCs examined in this study, $\min(f(t_s)) = f(0)$ and $\max(f(t_s)) = f(P_0)$. Thus we restate Eqs. 8 and 9 as

$$\tau > P_0 + f(0) \tag{10}$$

$$\tau < P_0 + f(P_0). \tag{11}$$

The following two equations define the allowable phases of the limit cycle where stable 1:1 phase locking may occur (Perkel et al., 1964) within the range of periods defined by Eqs. 10 and 11.

$$\frac{df(t_s)}{dt_s} > 0 \tag{12}$$

$$\frac{df(t_s)}{dt_s} < 2. \tag{13}$$

In summary, Eqs. 10 and 11 show that the PRC defines the possible range of frequencies for 1:1 phase locking. Equations 12 and 13 show that the slope of the PRC defines the phases (and the corresponding periods) where the 1:1 phase locking will be stable.

PRCs were generated for 2-nA hyperpolarizing inputs 0.5, 1, 2, 3, 5, and 10 s in duration, as well as the four types of synaptic input. These are the same inputs used for the entrainment diagram of Fig. 8. For each PRC the slope was numerically computed using a first-order central difference scheme. For each PRC the slope was numerically computed using a first-order central difference scheme. For all the PRCs investigated, the slope of the PRC was almost always positive or near zero. For each PRC the range of 1:1 entrainment periods that satisfied Eqs. 10–13 were defined by the following equation:

$$P_0 + f(t_{lim}) \le \tau < P_0 + f(P_0), \tag{14}$$

where t_{lim} was a minimal value of t_s, below which the slope of the PRC was always less than 2. Although some PRCs (e.g., Fig. 3 *B1*) had a region of negative slope, this did not affect the range of entrainable periods (although it did affect the range of entrainable phases). Assuming that subsequent cycles after the perturbation have a period of P_0, Eq. 14 may be modified to predict regions of stable 1:m entrainment (Moore et al., 1963) as follows:

$$mP_0 + f(t_{lim}) \le \tau < mP_0 + f(P_0). \tag{15}$$

The predicted regions of stable 1:m phase-locked entrainment are represented in Fig. 8 by the shaded regions, which should be compared with the simulated results indicated by the open circles.

The 1:m entrainment zones for the short-duration inputs in Fig. 8 are discontinuous, separated by regions of 2:m entrainment. This follows from Eq. 15. For the short duration inputs, there existed a region of the PRC corresponding to approximately 75% of the burst phase (interval I) where the slope of the PRC was greater than 2. The corresponding value of t_{lim} was typically between 1.5 and 2.0 s, so the ranges of τ predicted by Eq. 15 were discontinuous for successive values of m. It is in these discontinuous regions that 2:m entrainment zones were found. However, in the case of the long-duration inputs the slopes of the PRCs were always less than 2 for all values of t_s; thus $t_{lim} = 0$. Because $f(P_0) = P_0 + f(0)$, the ranges of stable entrainment for each m are given by $mP_0 + f(0) \le \tau \le (m + 1)P_0 + f(0)$. These ranges of τ are continuous for successive integer values of m, and noninteger entrainment zones do not exist. The lower limit of each entrainment zone for the short-duration inputs was longer than predicted if one included regions of 2:2m and 3:3m entrainment.

Comparison of the predicted versus simulated ECs suggests that the PRCs of the model are sufficient to predict zones of stable phase-locked entrainment of the model to periodic input. In addition, the current pulse ECs (Fig. 8, *A1* and *B1*) are similar to the corresponding synaptic input ECs (Fig. 8, *A2* and *B2*).

DISCUSSION

Comparison with previous studies

Aplysia LUQ neurons

The PRCs studied in the paper are similar to those found in R15 (H. Lechner, D. Baxter, and J. Byrne, personal communication). The most extensive studies of the phase sensitivity of bursting neurons have been made by Pinsker (1977a, b), who studied the phase sensitivity and entrainment properties of the left-upper-quadrant (LUQ) bursting neurons (primarily neuron L3) in the abdominal ganglion of *Aplysia*. These neurons are believed to burst in a manner similar to that of neuron R15 (Alevizos et al., 1991). The PRCs of the LUQ neurons were determined in response to both extrinsic current pulses and in response to IPSPs from the presynaptic neuron L10. Regions of phase advance and phase delay in the bursting neuron's PRC correspond to the ability of the neuron to be entrained by a stimulus pulse at periods shorter and longer (respectively) than the neuron's free running control period (Pinsker, 1977b). However, the PRCs were not related to the entrainment properties of the neuron in a quantitative manner, as was done by Perkel et al. (1964) for beating *Aplysia* neurons.

Figure 9 *F* of Pinsker (1977a) illustrates experimentally obtained PRCs of neuron L3 determined by current pulses and synaptic inputs (via stimulation of the presynaptic neuron L10). These PRCs are similar in shape to those obtained from our model by short current pulses and the medium and long synaptic models. Two of the findings of Pinsker (1977a) regarding the PRCs were that 1) the shape of the PRC remained constant when the duration of the presynaptic stimulus was changed and 2) the shape of the PRC was changed when short current pulses were applied directly to the cell. The results of this modeling study provide explanations for both of these findings.

In our simulations of synaptic input, we had precise control over the peak magnitude (via $\bar{g}_{syn}$) and duration (via k_r) of the synaptic conductance. However, in vitro Pinsker (1977a) could only control the duration of the synaptic input by lengthening the period of presynaptic activity. Our modeling studies indicate that such a procedure would only change the peak conductance of I_{syn} (via summation of transmitter pulses by g_{syn}) but will not change the channel's kinetics. The shape of the PRC and duration of I_{syn} are determined by the kinetics of I_{syn}. Thus it is expected that PRCs obtained via synaptic input would have the same shape, regardless of the duration of the presynaptic spike train. The duration of the input would simply shift the PRC upward.

Pinsker (1977a) also found that the PRC in response to a short current pulse input has a shape that is dramatically different from that of the PRC in response to synaptic input of a similar duration. According to our model, when a burst of spikes of a given duration is elicited in a presynaptic neuron (L10), the kinetics of g_{syn} would cause the resulting postsynaptic current to be much longer in duration than the applied input (see Fig. 6). This is consistent with the recording illustrated in figure 9 *A* of Pinsker (1977a), in which a 2-s presynaptic burst evoked an IPSP in neuron L3 approximately 8 s in duration. Thus it is inappropriate to compare the cell's response to a presynaptic burst of action potentials with an applied rectangular current pulse of duration similar to that of the burst. The results of our simulations suggest that longer square current pulses would elicit PRCs similar in shape to those obtained by synaptic input.

Although the relationship between PRCs and the ability to entrain a bursting neuron at periods shorter and longer than the neuron's free running frequency has been examined (Pinsker, 1977a, b), little or no work has been done (computationally or experimentally) to investigate quantitatively the entrainment properties of an endogenously bursting neuron. In the present study we found that for both the synaptic or current pulse inputs, regardless of duration, the predictions of the regions of phase-locked 1:*m* entrainment from the PRCs were in close agreement with those found via simulation. Furthermore, we found that for short inputs noninteger entrainment regions existed, and the location of these regions corresponded with those locations where the PRC predicted that stable phase-locked 1:*m* entrainment could not occur. These findings have not yet been investigated in vitro.

Other systems

Numerous experimental and computational studies have been made of the properties of entrainment and phase sensitivity of beating cells. These include the previously mentioned experimental study by Perkel et al. (1964), an experimental study of a time comparison circuit in the electric fish (Wessel, 1995), and experimental (Guttman et al., 1980) and computational (Best, 1979; Nemoto et al., 1975) studies of the squid axon. However, the most comprehensive studies of phase sensitivity and entrainment have been made on cardiac pacemakers (see Kowtha et al., 1994, for a review).

Two findings of the present study differentiate it from studies of cardiac pacemakers and beating neurons. First, all of the previous studies noted that phase sensitivity and entrainment properties of those cells were strongly dependent on the amplitude of the stimulus. This observation is in contrast with the present results, which indicate a minimal effect of amplitude on the characteristics of the PRC. Second, we investigated the effects of stimulus duration, which were not investigated previously, and found that noninstantaneous stimuli (i.e., those with a duration that was a noticeable fraction of the burst cycle) also resulted in nonlinear PRCs. These nonlinear PRCs, derived from long-duration inputs, were still relatively accurate at predicting the zones of 1:*m* entrainment by periodic input.

Comparison with circle model analysis

The problem of phase resetting has been of interest to theorists for many years (Pavlidis, 1973; Glass and Mackey, 1988; Winfree, 1987). It has been ideally studied in the context of a circle model, which consists of a two-variable model (θ and r) whose limit cycle is represented in polar coordinates by a circle with the equilibrium point at its center. Thus the limit cycle oscillation consists of a time-varying θ with a constant radius r. According to this scheme, limit cycle models may exhibit two types of phase resetting, type 0 and type 1. A brief perturbation of the limit cycle C produces at perturbed limit cycle C', which may or may not enclose the origin. In type 1 (weak) resetting, the PTC has an average slope of 1 and C' encloses the origin. In type 0 (strong) resetting, the PTC has an average slope of 0 and C' does not enclose the origin.

In the context of our model, C and C' are analogous to the limit cycle and perturbed limit cycle, respectively. All of our PRCs/PTCs exhibit type 0 (strong) resetting, because the PTCs have an average slope of 0 (Fig. 3 *B1*). This is supported by the observation that in almost every case the perturbed limit cycles do not enclose the equilibrium point (Fig. 3, *B2–D2*), with the exception of the 1.6-nA, 1-s input (Fig. 3, *B2*), which marginally encloses the equilibrium point. The equilibrium point in Fig. 3, *B2–C2*, is the intersection of S_c and C_c in Fig. 5.

Clay et al. (1990) pointed out some weaknesses of the circle model in the analysis of an ionic current-based model of chick atrial heart cells. Specifically, when examining the phase sensitivity of the model in terms of *I–V* plots, they found that there was not always a correlation between the character of the PTCs (type 1 or type 0), whether or not their perturbed limit cycles enclosed the equilibrium point. They attributed this discrepancy to two things: 1) their model contains many more variables than the ideal circle model, and 2) the relaxation of the model's solution trajectory after a perturbation back to the limit cycle does not occur instantaneously. In our model, the circle model analysis paradigm does seem to apply. We attribute this to two things: 1) our study only examines the effects of hyperpolarizing stimuli, and at hyperpolarized potentials the model dynamically collapses to a second-order system (Butera et al., 1996); and 2) although the model does not relax back to the limit cycle immediately, such relaxation is complete or nearly complete (for pulses applied in interval III) by the time the period measurement is made.

We wish to express our gratitude to D. A. Baxter, C. C. Canavier, and H. Lechner for helpful discussions, and to Ron Dror for providing critical readings of the manuscript. We thank the reviewers for their insights, which improved the content of the manuscript.

This work was supported by Office of Naval Research grant N00014-92-1152 (JHB and JWC), NIMH Award K05 MH 00649 (JHB), and a Whitaker Foundation Graduate Fellowship in Biomedical Engineering (RJB).

APPENDIX: EQUATIONS AND PARAMETERS OF THE MODEL

This appendix contains the equations and values of parameters of the model not already listed in the text. In these equations, time is in ms, current is in nA, potential is in mV, and concentrations are in mM.

I_{Na}: fast sodium current

$$I_{Na} = \bar{g}_{Na} m^3 h (V - E_{Na})$$

$$m_\infty(V) = \frac{1}{1 + \exp((-10.23 - V)/10.0)}$$

$$\tau_m(V) = 1/(A_m(V) + B_m(V))$$

$$A_m(V) = \frac{0.40(V + 6.0)}{1 - \exp((-V - 6.0)/4.09)}$$

$$B_m(V) = 10.75 \exp((-28.0 - V)/4.01)$$

$$h_\infty(V) = \frac{1}{1 + \exp((V + 25.0)/3.0)}$$

$$\tau_h(V) = 1/(A_h(V) + B_h(V))$$

$$A_h(V) = 0.067 \exp((-43.0 - V)/25.0)$$

$$B_h(V) = \frac{0.307}{1 + \exp((12.65 - V)/23.9)}$$

I_{Ca}: fast calcium current

$$I_{Ca} = \bar{g}_{Ca} \frac{1}{1 + \exp((c - K_{Ca})/D_{Ca})} d^2 f (V - E_{Ca})$$

$$d_\infty(V) = \frac{1}{1 + \exp((10.0 - V)/3.8)}$$

$$\tau_d(V) = 1/(A_d(V) + B_d(V))$$

$$A_d(V) = \frac{0.0063(V + 10.81)}{1 - \exp((-V - 10.81)/5.03)}$$

$$B_d(V) = 0.01 \exp((25.0 - V)/10.0)$$

$$f_\infty(V) = \frac{1}{1 + \exp((V + 20.0)/4.0)}$$

$$\tau_f(V) = 1/(A_f(V) + B_f(V))$$

$$A_f(V) = 0.00325 \exp((10.0 - V)/7.57)$$

$$B_f(V) = \frac{0.029}{1 + \exp((20.29 - V)/5.4)}$$

I_{SI}: slow inward calcium current

$$I_{SI} = \bar{g}_{SI}\left(\frac{K_{SI,Ca}}{K_{SI,Ca} + c}\right)s(V - E_{Ca})$$

$$s_\infty(V) = \frac{1}{1 + \exp((-40.0 - V)/11.5)}$$

$$\tau_s(V) = 1/(A_s(V) + B_s(V))$$

$$A_s(V) = \frac{0.0014(V - 54.0)}{1 - \exp((-V + 54.0)/12.63)}$$

$$B_s(V) = 0.00013\exp((-11.32 - V)/16.8)$$

I_{NS}: nonspecific cation current

$$I_{NS} = \bar{g}_{NS}\left(\frac{c}{c + K_{NS,Ca}}\right)b(V - E_{NS})$$

$$\tau_b(V) = 500\left(\frac{0.80}{1 + \exp((10.0 + V)/3.0)} + 0.20\right)$$

$$I_{NS,Ca} = 0.197 I_{NS}\frac{V - E_{Ca}}{V - E_{NS}}$$

I_L: leakage current

$$I_L = \bar{g}_L(V - E_L)$$

I_K: delayed rectifier

$$I_K = \bar{g}_K n^4 l(V - E_K)$$

$$n_\infty(V) = \frac{1}{1 + \exp((3.65 - V)/14.46)}$$

$$\tau_n(V) = 1/(A_n(V) + B_n(V))$$

$$A_n(V) = \frac{0.0035(V + 17.0)}{1 - \exp((-V - 17.0)/3.0)}$$

$$B_n(V) = 0.04\exp((-28.0 - V)/10.0)$$

$$l_\infty(V) = \frac{1}{1 + \exp((32.5 + V)/12.7)}$$

$$\tau_l(V) = 2000\left(\frac{0.90}{1 + \exp((28.0 + V)/3.0)} + 0.10\right)$$

I_R: anomalous rectifier

$$I_R = \bar{g}_R\frac{(V - E_K + 5.66)}{1 + \exp((V - E_K - 15.3)ZF/RT)}$$

Pumps and exchangers

$$I_{CaP} = \bar{I}_{CaP}\left(\frac{c}{c + K_{P,Ca}}\right)$$

$$I_{NaK} = \bar{I}_{NaK}\left(\frac{[Na]_i}{[Na]_i + K_{P,Na}}\right)^3\left(\frac{[K]_0}{[K]_0 + K_{P,K}}\right)^2 \times \left(\frac{1.5}{1.5 + \exp\left(\frac{-V-60}{40}\right)}\right)$$

$$I_{NaCa} = K_{NaCa}(DF_{in} - DF_{out})/S$$

$$S \equiv 1 + D_{NaCa}([Ca]_i[Na]_0^r + [Ca]_0[Na]_i^r)$$

$$DF_{in} \equiv [Na]_i^r[Ca]_0\exp\left(\frac{(r-2)\gamma VF}{RT}\right)$$

$$DF_{out} \equiv [Na]_0^r[Ca]_i\exp\left(\frac{(r-2)(\gamma-1)VF}{RT}\right)$$

Parameters

C_M	=	17.5 nF
$\bar{g}_{Na}$	=	38 μS
$\bar{g}_{Ca}$	=	17 μS
$\bar{g}_K$	=	70 μS
$\bar{g}_{NS}$	=	0.2 μS
$\bar{g}_{SI}$	=	0.65 μS
$\bar{g}_R$	=	0.315 μS
$\bar{g}_L$	=	0.075 μS
E_{Na}	=	54 mV
E_{Ca}	=	65 mV
E_K	=	−77 mV
E_{NS}	=	−22 mV
E_L	=	10.3 mV
$[Na]_0$	=	500 mM
$[Na]_i$	=	50 mM
$[K]_0$	=	10 mM
$[Ca]_0$	=	10 mM
$[B]_i$	=	112.5×10^{-3} mM
$\bar{I}_{CaP}$	=	7.0 nA
$\bar{I}_{NaK}$	=	7.7 nA
K_{NaCa}	=	0.01
D_{NaCa}	=	0.01
γ	=	0.5
r	=	4
R	=	8,314 J/kg mol °K
F	=	96,500 C/mol
T	=	295 °K
Z	=	2
Vol_i	=	4.0 nl
k_U	=	100 mM^{-1} ms^{-1}
k_R	=	0.238 ms^{-1}
n_B	=	4
$K_{SI,Ca}$	=	25×10^{-6} mM

$$K_{NS,Ca} = 150 \times 10^{-6}\ mM$$
$$K_{P,Ca} = 350 \times 10^{-6}\ mM$$
$$K_{P,Na} = 5.46\ mM$$
$$K_{P,K} = 0.621\ mM$$
$$K_{Ca} = 0.5 \times 10^{-3}\ mM$$
$$D_{Ca} = 0.15 \times 10^{-3}\ mM$$

REFERENCES

Adams, W. B., and J. A. Benson. 1985. The generation and modulation of endogenous rhythmicity in the *Aplysia* bursting pacemaker neurone R15. *Prog. Biophys. Mol. Biol.* 46:1–49.

Alevizos, A., M. Skelton, K. R. Weiss, and J. Koester. 1991. A comparison of bursting neurons in *Aplysia*. *Biol. Bull.* 180:269–275.

Aschoff, J., editor. 1965. Circadian Clocks. North Holland Publishing Co., Amsterdam.

Best, E. N. 1979. Null space in the Hodgkin-Huxley equations: a critical test. *Biophys. J.* 27:87–104.

Brown, G., and J. Eccles. 1934. The action of a single vagal volley on the rhythm of the heart beat. *J. Physiol. (Lond.).* 82:211–241.

Butera, R. J., J. W. Clark, and J. H. Byrne. 1996. Dissection and reduction of a modeled bursting neuron. *J. Computat. Neurosci.* 3:199–223.

Butera, R. J., J. W. Clark, C. C. Canavier, D. A. Baxter, and J. H. Byrne. 1995. Analysis of the effects of modulatory agents on a modeled bursting neuron: dynamic interactions between voltage and calcium dependent systems. *J. Computat. Neurosci.* 2:19–44.

Clay, J. R., R. M. Brochu, and A. Shrier. 1990. Phase resetting of embryonic chick atrial heart cell aggregates. *Biophys. J.* 58:609–621.

Doedel, E. J. 1981. AUTO: a program for the automatic bifurcation and analysis of autonomous systems. *Congressus Numerantium.* 30: 265–284.

Dong, E., and B. A. Reitz. 1970. Effect of timing of vagal stimulation on heart rate in the dog. *Circ. Res.* 27:635–646.

Enright, J. T. 1965. Synchronization and ranges of entrainment. *In* Circadian Clocks. J. Aschoff, editor. North Holland, Amsterdam. 112–124.

Gardner, D., and C. F. Stevens. 1980. Rate-limiting step of inhibitory post-synaptic current decay in *Aplysia* buccal ganglia. *J. Physiol. (Lond.).* 304:145–164.

Glass, L., and M. Mackey. 1988. From Clocks to Chaos: The Rhythms of Life. Princeton University Press, Princeton, NJ.

Guevera, M. R., A. Shrier, and L. Glass. 1988. Phase-locked rhythms in periodically stimulated heart cell aggregates. *Am. J. Physiol.* 254: H1–H10.

Guttman, R., L. Feldman, and E. Jakobsson. 1980. Frequency entrainment of squid axon membrane. *J. Membr. Biol.* 59:9–18.

Hairer, E., and G. Wanner. 1990. Solving Ordinary Differential Equations. II. Stiff and Differential-Algebraic Problems. Springer Series in Computational Mathematics. Springer-Verlag, New York.

Jalife, J., and G. K. Moe. 1976. Effect of electrotonic potentials in pacemaker activity of canine purkinje fibers in relation to parasystole. *Circ. Res.* 39:801–808.

Kowtha, V. C., A. Kunysz, J. R. Clay, L. Glass, and A. Shrier. 1994. Ionic mechanisms and nonlinear dynamics of embryonic chick heart cell aggregates. *Prog. Biophys. Mol. Biol.* 61:255–281.

Levy, M. N., P. J. Martin, and T. Iaona. 1969. Paradoxical effect of vagus nerve stimulation on the heart. *Circ. Res.* 25:303–314.

Magleby, K. L., and C. F. Stevens. 1972. A quantitative description of end-plate currents. *J. Physiol. (Lond.).* 223:173–197.

Moore, G. P., D. H. Perkel, and J. P. Segundo. 1963. Stability patterns in interneuronal pacemaker regulation. *Proc. San Diego Symp. Biomed. Eng.* 184–193.

Nemoto, I., S. Miyazaki, M. Saito, and T. Utsunomiya. 1975. Behavior of solutions of the Hodgkin-Huxley equations and its relation to properties of mechanoreceptors. *Biophys. J.* 15:469–479.

Pavlidis, T. 1973. Biological Oscillators: Their Mathematical Analysis. Academic Press, New York.

Perkel, D. H., J. H. Schulman, and T. H. Bullock. 1964. Pacemaker neurons: effect of regularly spaced synaptic input. *Science.* 145:61–63.

Pinsker, H. M. 1977a. *Aplysia* bursting neurons as endogenous oscillators. I. Phase-response curves for pulsed inhibitory synaptic input. *J. Neurophysiol.* 40:527–543.

Pinsker, H. M. 1977b. *Aplysia* bursting neurons as endogenous oscillators. II. Synchronization and entrainment by pulsed inhibitory synaptic input. *J. Neurophysiol.* 40:544–556.

Reid, J. V. O. 1969. The cardiac pacemaker: effects of regularly spaced nervous input. *Am. Heart J.* 78:58–64.

Rheinboldt, W., and J. Burkardt. 1983a. Algorithm 596: a program for a locally parameterized continuation process. *ACM Trans. Math. Software.* 9:236–241.

Rheinboldt, W., and J. Burkardt. 1983b. A locally parameterized continuation process. *ACM Trans. Math. Software.* 9:215–235.

Weidmann, S. 1951. Effect of current flow on the membrane potential of cardiac muscle. *J. Physiol. (Lond.).* 115:227–236.

Wessel, R. 1995. In vitro study of phase resetting and phase locking in a time-comparison circuit in the electric fish. *Eigenmannia. Biophys. J.* 69:1880–1990.

Winfree, A. T. 1987. The Timing of Biological Clocks. Scientific American Books, New York.